Adaptive Path-Following Control For Ground Vehicles Using A Switching Non-Quadratic Lyapunov Function

Xingyu Zhou*, Zejiang Wang†, and Junmin Wang*
*Walker Department of Mechanical Engineering, University of Texas at Austin, Austin, TX, USA
†Oak Ridge National Laboratory, Oak Ridge, TN, USA
Email: {xingyu.zhou, jwang}@austin.utexas.edu, wangz2@ornl.gov

***Abstract*— The application of adaptive control techniques in the development of control systems for intelligent vehicles, especially for ground vehicle path-following controllers, has gained popularity due to their ability to handle large-scale parametric uncertainties. However, the use of a standard quadratic Lyapunov function in existing adaptive control-based path-following controllers can lead to poor transient performance, such as slow convergence and/or large overshoot. To address this limitation, this study proposes the use of a switching non-quadratic Lyapunov function to design a model reference adaptive path-following controller that aims to provide superior transient performance. The stability and signal convergence of the closed-loop system are demonstrated through a Lyapunov-like analysis. Through dSPACE ASM simulation, the effectiveness of the proposed controller is illustrated, which confirms improved tracking performance over a baseline solution.**

Keywords—Adaptive Control, Autonomous Driving, Path Following, Switching Non-Quadratic Lyapunov Function

I. INTRODUCTION

A. Background

In recent times, the development of modern intelligent vehicles (IV) has been greatly propelled by the synergy of cutting-edge hardware, software, and artificial intelligence [1], [2]. Notably, autonomous/automated driving systems (ADS), the backbone technology of IV, have gained significant attention due to their numerous societal and economic benefits [3]. Among the foundational subsystems of ADS, the path-following control design has emerged as a critical research area.

In essence, the path-following control system is responsible for guiding a vehicle to follow a dynamically feasible path produced by the path-planning subsystem [4]. As a primary design objective, the lateral and heading errors with respect to the reference path shall be regulated as small as possible for a good tracking performance [4]. Typically, the design of the path-following control system relies on a process dynamic model (*e.g.*, the vehicle lateral dynamic model). However, model uncertainties, especially (large-scale) parametric uncertainties, make this task challenging. As reported in [5],[6], vehicle parameters, such as tire stiffness and payload mass, are contingent on both vehicle configurations and environmental factors, rendering them subject to variation over time and from vehicle to vehicle. Inadequate compensation of these uncertainties may result in degradation of the tracking performance and, in severe cases, destabilization of the closed-loop system. Therefore, it is crucial to address parametric uncertainties with caution when developing a path-following control system.

B. Literature Overview

When it comes to dealing with parametric uncertainties in vehicle dynamic models, two general approaches for controller synthesis exist. The first is the robust control (RC) theory, which aims to stabilize the closed-loop system under worst-case model parameter uncertainties with fixed control laws (see [7] and references therein). The second approach hinges upon the adaptive control (AC) method, which yields online adjusted control strategies and may offer two advantages over RC (see [8] and references therein). First off, the RC method requires prior knowledge of the uncertain model parameter bounds, while AC does not rely on such information and is capable of intelligently identifying and learning the model parameters in real-time. Secondly, large-scale parametric uncertainties can induce conservative control laws with RC synthesis. Such conservativeness may result in excessively large control effort and/or inadequate performance [9], which may be unsuitable for the path-following control system. In contrast, the AC framework does not have this drawback.

In this respect, a multitude of research efforts has focused on developing path-following controllers leveraging the AC theory. For instance, ref. [8],[10],[11] utilized the model reference adaptive control (MRAC) design to synthesize path-following controllers. More recently, Lyapunov-based adaptation mechanisms have been synergized with various emergent path-following control methods, leading to the development of the adaptive data-driven controller [1], the adaptive model predictive controller [12], the adaptive steering-backlash compensator [13], among others.

C. Our Work's Novelty and Contribution

The mainstream adaptive path-following controllers for ground vehicles rely on quadratic Lyapunov functions (QLF) [8]. Although effective, these controllers can only guarantee global stability and signal boundedness of the closed-loop system in theory, and at best, can ensure asymptotic convergence of tracking errors. However, QLF-based solutions have been criticized for their arbitrary transient performance, which may exhibit sub-standard signs such as slow convergence of tracking errors and large over/undershoot.

To address the limitations of QLF-based controllers, this paper proposes a new method for achieving path-following targets in ground vehicles. The approach utilizes an MRAC with a *switching non-quadratic* Lyapunov function (SNQLF) design, which offers a core benefit over the conventional QLF counterpart. Specifically, the SNQLF design can dynamically improve the parameter-adaptation process, resulting in better tracking performance. Overall, the proposed path-following control strategy utilizes a hierarchical control structure that divides the control objective into two sub-levels: kinematic-error regulation and reference yaw-rate tracking. The high-level control module, which is based on H_∞ robust control theory, regulates kinematic tracking errors and generates a reference yaw rate trajectory (which serves as the virtual control input to the high-level control loop). The low-level control system, implemented as an SNQLF-based MRAC, is responsible for the reference yaw rate tracking. To further enhance both the robustness and efficiency of the parameter learning process, a projection scheme is integrated into the parameter update laws.

D. Paper Outline

A summary of the remaining sections of this paper is as follows. Section II introduces the system model and the design of the hierarchical control architecture. In Section III, a H_∞ robust controller is proposed as the high-level kinematic-error controller to regulate the lateral and yaw angle errors. Section IV delineates the development of the low-level SNQLF-based MRAC with a projection scheme to track the reference yaw rate trajectory. Section V presents the validation results using dSPACE ASM. Finally, Section VI provides the conclusion of this paper.

II. Modeling and Control System Design

This section provides an introduction to the kinematic error model for vehicle path following and the linear vehicle single-track model. Additionally, the design principles of the duo-loop hierarchical control architecture are presented.

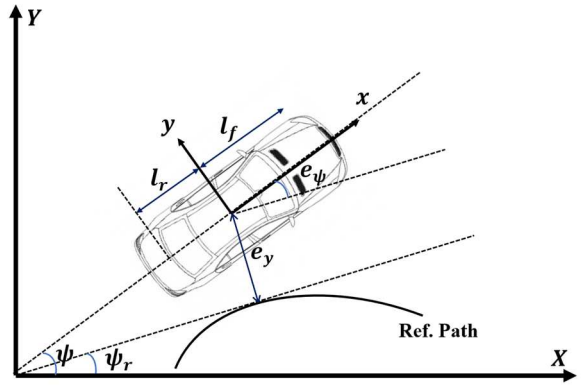

Figure 1. Path-following kinematics

A. Path-Following Kinematic Error Model

The nonlinear differential equations for the kinematic path-following error model are expressed as per [14]:

$$\begin{cases} \dot{e}_y = v_x \sin(e_\psi) + v_y \cos(e_\psi) \\ \dot{e}_\psi = \omega_z - \dot{\psi}_r \end{cases}. \quad (1)$$

As visualized in Figure 1, e_y represents the lateral error between the vehicle's COG and the reference path, e_ψ and $\dot{\psi}_r$ are the heading angle error and the reference yaw rate respectively, and ω_z is the vehicle yaw rate.

B. Linear Single-Track Vehicle Lateral Dynamics

Given the strong linearity of vehicle dynamics during normal driving conditions, it is sensible to model the vehicle's lateral dynamics with the well-known linear single-track model [15],[16]. The state vector of this model is given by $x = (\beta \quad \omega_z)^T$.

$$\dot{x} = Ax + B\delta, \quad (2)$$

where,

$$\begin{cases} A = \begin{pmatrix} -\dfrac{\mathcal{K}_f + \mathcal{K}_r}{mv_x} & -1 + \dfrac{l_r\mathcal{K}_r - l_f\mathcal{K}_f}{mv_x^2} \\ \dfrac{l_r\mathcal{K}_r - l_f\mathcal{K}_f}{I_z} & -\dfrac{l_r^2\mathcal{K}_r + l_f^2\mathcal{K}_f}{I_z v_x} \end{pmatrix}. \\ = \begin{pmatrix} \dfrac{\mathcal{K}_f}{mv_x} & \dfrac{l_f\mathcal{K}_f}{I_z} \end{pmatrix}^T \end{cases} \quad (3)$$

The linear single-track vehicle model in $(2)-(3)$ is characterized by the following parameters: the vehicle mass, denoted by m, the front and rear wheelbases, represented by l_f and l_r respectively, the tire cornering stiffness of the front and rear axles, denoted by $\mathcal{K}_f$ and $\mathcal{K}_r$ respectively, and the vehicle's yaw inertia, denoted by I_z. The control input for this model is the front road-wheel angle δ (so-called active front steering control).

C. Hierarchical Control Architecture

Inspired by [8], a hierarchical control framework is introduced, comprising a high-level kinematic-error regulator and a low-level controller for tracking the yaw rate reference trajectory produced by the former. The H_∞ robust control theory is utilized to design the high-level controller, which provides guaranteed L_2 -to- L_2 attenuation from external disturbances to the performance output. The low-level control system, on the other hand, is formulated as an SNQLF-based MRAC. Such a hierarchical control construction is suggested based on the following considerations: First off, as the kinematic errors in equation (1) are not subject to parametric uncertainties, controlling the path-following error vector $(y_e \quad \varphi_e)$ can be achieved through deterministic control laws, reducing the complexity of the adaptive system, and making the design and analysis of the adaptive control more feasible. Besides, some motion-planning modules documented in the literature can provide reference yaw rate trajectories directly, enabling our SNQLF-based MRAC to be employed straightforwardly for achieving yaw rate tracking.

III. H_∞ Robust Kinematic-Error Regulator

A H_∞ robust controller (for regulating path-following kinematic errors) is formulated in terms of linear matrix inequalities (LMI). Additionally, we consider the time-varying longitudinal velocity of the vehicle in the controller synthesis and employ a self-scheduling scheme to account for this.

A. H_∞ Robust Controller

Linearization of the nonlinear vehicle path-following

kinematic error model in (1) can be performed around the operating point $(y_e \quad \varphi_e) = (0 \quad 0)$, resulting in the following linear model:

$$\begin{pmatrix}\dot{e}_y\\ \dot{e}_\psi\end{pmatrix} = \begin{pmatrix}0 & v_x\\ 0 & 0\end{pmatrix}\begin{pmatrix}e_y\\ e_\psi\end{pmatrix} + \begin{pmatrix}0\\ 1\end{pmatrix}\omega_r + \begin{pmatrix}0\\ 1\end{pmatrix}\dot{\psi}_r$$
$$\Leftrightarrow \dot{\gamma} = A_e\gamma + B_e\omega_r + E_e\dot{\psi}_r. \quad (4)$$

In (4), it is assumed that the low-level yaw-rate servo loop has a sufficiently high bandwidth (with reference to the high-level control loop) such that $\omega_r \approx \omega_z$ (ω_r is treated as a virtual control input). For the robust control objective, the performance output is defined as $z \triangleq^{\text{def}} C_e\gamma$,

$$C_e = \begin{pmatrix}\Gamma_{e_y} & \Gamma_{e_\psi}\end{pmatrix}, \quad (5)$$

where $\Gamma_{y_e}, \Gamma_{y_e} \in \mathbb{R}^+$ are positive weighting factors. The primary aim of the state-feedback H_∞ robust controller, which operates with $\omega_r = K\gamma + v_x\kappa$, is to minimize the energy-to-energy induced gain from $\dot{\psi}_r$ to the performance output z, while satisfying other constraints. In other words, across the entire frequency spectrum of $\dot{\psi}_r$, the devised H_∞ can ensure the least sensitivity from $\|\dot{\psi}_r\|_2$ to $\|z\|_2$. Prior to deriving the H_∞ robust controller, a lemma is presented as follows regarding the LMI-based eigenvalue assignment. The eigenvalue assignment criterion is implemented in the robust controller synthesis to shape the high-level control loop's transient performance as well as restrain its bandwidth.

Lemma 1. [17] For a linear-time-invariant (LTI) system governed by $\dot{\eta} = N\eta$ where $N \in \mathbb{R}^{n\times n}, \eta \in \mathbb{R}^n$, all of its eigenvalues lie inside a circular region $\mathcal{C}$ with a radius of r (in the complex plane) and centered around $c \in \mathbb{C}^2$ if and only if $\exists\, M \in \mathbb{S}^n_{++}$ such that,

$$\begin{pmatrix}-rM & cM + MN\\ * & -rM\end{pmatrix} < 0. \quad (6)$$

More explicitly, the circular region $\mathcal{C}$ is characterized by,

$$\mathcal{C} = \{p \in \mathbb{C}^2 : \|p + c\| < r\}, \quad (7)$$

Theorem 1. $\|T_{\dot{\psi}_r\to z}\|_{H_\infty} < \epsilon \in \mathbb{R}^+ \left(\|z\|_{L_2} < \lambda\|d\|_{L_2}\right)$ and all closed-loop poles are enclosed inside the region $\mathcal{C}$ if and only if $\exists\, X \in \mathbb{S}^2_{++}, \epsilon \in \mathbb{R}^+$ such that,

$$\begin{cases}\begin{pmatrix}\mathcal{H}[A_eX + B_eY] & E_e & XC_e^T\\ * & -\epsilon I & 0\\ * & * & -\epsilon I\end{pmatrix} < 0\\ \begin{pmatrix}-rX & cX + A_eX + B_eY\\ * & -rX\end{pmatrix} < 0\end{cases}, \quad (8)$$

where $\mathcal{H}(\bullet) \triangleq^{\text{def}} \bullet + \bullet^T$.

Proof:

Applying the Kalman–Yakubovich–Popov lemma in [17], the criterion $\|T_{\dot{\psi}_r\to z}\|_{H_\infty} < \epsilon \in \mathbb{R}^+$ is satisfied if and only if $\exists\, P \in \mathbb{S}^2_{++}$ and $\epsilon \in \mathbb{R}^+$ such that,

$$\begin{pmatrix}\mathcal{H}[P(A_e + B_eK)] & PE_e & C_e^T\\ * & -\epsilon I & 0\\ * & * & -\epsilon I\end{pmatrix} < 0. \quad (9)$$

Through multiplying $\mathrm{diag}(P^{-1}, I, I)$ on both sides of (9) and encoding $P^{-1} = X$, $KX = Y$, the first LMI in (8) is established.

Next, the criterion for $\mathcal{C}$-regional eigenvalue placement, as described in Lemma 1, states that all the closed-loop eigenvalues are located within $\mathcal{C}$ if and only if there exists a matrix $\exists\, M \in \mathbb{S}^2_{++}$ satisfying the LMI,

$$\begin{pmatrix}-rM & cM + M(A_k + B_kK)\\ * & -rM\end{pmatrix} < 0. \quad (10)$$

Accordingly, the second LMI in (8) can be established by applying another congruent transformation on (10), which involves multiplying both sides by $\mathrm{diag}(M^{-1}, M^{-1})$, and then making the change-of-variables $M^{-1} = X$ and $KX = Y$.

The H_∞ robust control gain K matrix can be carried out by,

$$K = YX^{-1}. \quad (11)$$

This completes the proof for Theorem 1. ■

B. Self-Scheduling Scheme

The proposed H_∞ robust control law at its current state considers v_x being constant. However, to maintain the closed-loop robust stability in the presence of potentially time-varying v_x, modifying the feedback control gain K is required to account for variations in v_x. One effective way is to adopt a polytopic gain-scheduling approach, where v_x is regarded as a measurable scheduling signal. Assuming v_x is enclosed inside the interval,

$$v_x \in [\underline{v}_x \quad \overline{v}_x],\ \underline{v}_x \in \mathbb{R}^+, \quad (12)$$

the state-space form $T(v_x)$ of the closed-loop system can be expressed as a convex combination of individual state-space realizations at two interval endpoints, i.e.,

$$T(v_x) = \underline{\varepsilon}T(\underline{v}_x) + \overline{\varepsilon}T(\overline{v}_x). \quad (13)$$

Factors $\underline{\varepsilon}$ and $\overline{\varepsilon}$ can be carried out as,

$$\underline{\varepsilon} \triangleq^{\text{def}} \frac{\overline{v}_x - v_x}{\overline{v}_x - \underline{v}_x}, \overline{\varepsilon} \triangleq^{\text{def}} \frac{v_x - \underline{v}_x}{\overline{v}_x - \underline{v}_x}. \quad (14)$$

Thus, the self-scheduled (respecting v_x) feedback control gain K is acquired as the convex sum of control gain matrices $K(\underline{v}_x)$ and $K(\overline{v}_x)$, which are synthesized with identical X (to ensure the quadratic stability of the closed-loop system against the bounded v_x) at the endpoints $\underline{v}_x$ and $\overline{v}_x$, i.e.,

$$K = \underline{\kappa}K(\underline{v}_x) + \overline{\kappa}K(\overline{v}_x). \quad (15)$$

IV. SNQLF-MRAC Synthesis

This section presents the design of an output-feedback MRAC using SNQLF, aimed at achieving asymptotic tracking of the yaw rate reference command produced by the high-level H_∞ robust kinematic-error controller. Additionally, an analysis of the adaptive closed-loop system's stability and signal convergence is presented.

A. Linear Single-Track Vehicle Lateral Dynamic Model

The linear state-space representation as in (2) − (3) can be readily converted to a transfer function ($s \in \mathbb{C}$ is the Laplace variable):

$$T_{\delta\to\omega_z} = \frac{\begin{vmatrix} mv_xs + \mathcal{K}_f + \mathcal{K}_r & \mathcal{K}_f\\ l_f\mathcal{K}_f - l_r\mathcal{K}_r & l_f\mathcal{K}_f\end{vmatrix}}{\begin{vmatrix} mv_xs + \mathcal{K}_f + \mathcal{K}_r & mv_x + \dfrac{(l_f\mathcal{K}_f - l_r\mathcal{K}_r)}{v_x}\\ l_f\mathcal{K}_f - l_r\mathcal{K}_r & I_zs + \dfrac{(l_f^2\mathcal{K}_f - l_r^2\mathcal{K}_r)}{v_x}\end{vmatrix}}. \quad (16)$$

In line with [8], the subsequent variables are designated as follows,

$$\begin{cases} \mathcal{S} \triangleq -\frac{m(l_f\mathcal{K}_f - l_r\mathcal{K}_r)}{(l_f+l_r)^2\mathcal{K}_f\mathcal{K}_r} \\ \omega_n \triangleq \frac{(l_f+l_r)}{v_x}\sqrt{\frac{\mathcal{K}_f\mathcal{K}_r}{mI_z}(1+\mathcal{Z}v_x^2)} \\ \zeta \triangleq \frac{m\left(l_f^2\mathcal{K}_f + l_r^2\mathcal{K}_r\right) + I_z(\mathcal{K}_f+\mathcal{K}_r)}{2(l_f+l_r)\sqrt{mI_z\mathcal{K}_f\mathcal{K}_r(1+\mathcal{Z}v_x^2)}} \end{cases}. \quad (17)$$

By utilizing the stability factor $\mathcal{S}$, natural frequency ω_n, and damping ratio ζ, as defined in (17), the transfer function in (16) can be simplified as follows:

$$T_{\delta\to\omega_z} = \mathcal{K}_h\frac{s+T_z^{-1}}{s^2+2\zeta\omega_n s+\omega_n^2} = \mathcal{K}_h\frac{P_n}{P_d}. \quad (18)$$

The transfer function's high-frequency gain is denoted as $\mathcal{K}_h \triangleq \frac{v_x T_z \omega_n^2}{(1+\mathcal{S}v_x^2)(l_f+l_r)}$, and the time constant of the $T_{\delta\to\omega_z}$'s zero dynamics is symbolized as $T_z \triangleq \frac{ml_f v_x}{\mathcal{K}_r(l_f+l_r)}$. It is reasonable to assume the vehicle is under-steered (i.e., $\mathcal{S}\in\mathbb{R}^+$) as most commercial vehicle manufacturers design their vehicles this way [15]. As a result, the transfer function is minimum-phase and has a relative degree of one. In addition, the sign of the high-frequency gain $\mathcal{K}_h$ is always positive. Based on these facts, the following certainty-equivalence MRAC law can be employed to achieve the yaw-rate tracking objective:

$$\delta = \hat{\theta}_k\omega_r + \hat{\theta}_0\omega_z + \hat{\theta}_1\mathcal{T}_1 + \hat{\theta}_2\mathcal{T}_2, \quad (19)$$

where $\widehat{\Theta} \triangleq (\hat{\theta}_k \quad \hat{\theta}_0 \quad \hat{\theta}_1 \quad \hat{\theta}_2)^T \in \mathbb{R}^4$ are estimated control parameters (their update laws are to be derived), $\mathcal{T}_1$ and $\mathcal{T}_2$ are two auxiliary signals acquired through low-pass filtering δ and ω_z respectively,

$$\begin{cases} \mathcal{T}_1(s) = \mathcal{F}_1(s)\delta(s) \\ \mathcal{T}_2(s) = \mathcal{F}_2(s)\omega_z(s) \end{cases}. \quad (20)$$

Transfer functions for these exponentially stable low-pass filters (as $\rho\in\mathbb{R}^+$) can be designed identically ($\kappa\in\mathbb{R}^+$),

$$\mathcal{F}_1(s) = \mathcal{F}_2(s) = \frac{\lambda_n}{\lambda_d} = \frac{\kappa}{s+\rho}. \quad (21)$$

The reference model's transfer function can be designed as,

$$T_{\omega_r\to\omega_m} = \frac{1}{\frac{s}{a_m}+1} = \frac{1}{R_r} \quad (22)$$

where $a_m\in\mathbb{R}^+$ is the reference model's bandwidth.

According to the MRAC design's matching condition, $\exists\,\Theta \triangleq (\theta_k \quad \theta_0 \quad \theta_1 \quad \theta_2)^T \in \mathbb{R}^4$ such that,

$$\begin{aligned}&(\theta_0\lambda_d + \theta_2\lambda_n)\mathcal{K}_h P_n + \theta_1\lambda_n P_d \\ &= -\lambda_d(\theta_k\mathcal{K}_h\lambda_n R_r - P_d).\end{aligned} \quad (23)$$

When Θ is perfectly known, i.e., $\widehat{\Theta}=\Theta$, the MRAC proposed in (19) reduces to a deterministic model-reference controller (DMRC). The DMRC can guarantee that the yaw-rate tracking error ($\omega_e \triangleq \omega_z - \omega_m$, defined as the difference between the output of the reference model (ω_m) and the actual output (ω_z) converges to zero exponentially fast, namely,

$$\omega_e(t) = \omega_e(t_0)\exp[-a_m(t-t_0)], \forall t\geq t_0. \quad (24)$$

However, in practical applications, it is rare for Θ to be precisely known and it may be subject to variations over time. To address such parametric uncertainties, a real-time adaptation scheme based on a projection-modified SNQLF is proposed to learn Θ: $\forall\, i = k, 0, 1, 2$,

$$\hat{\theta}_i = \mathrm{Proj}_{[\underline{\theta}_i,\overline{\theta}_i]}(\breve{\theta}_i) = \begin{cases} \breve{\theta}_i, \forall\,\breve{\theta}_i \in (\underline{\theta}_i, \overline{\theta}_i) \\ \underline{\theta}_i, \forall\,\breve{\theta}_i \in (-\infty, \underline{\theta}_i), \\ \overline{\theta}_i, \forall\,\breve{\theta}_i \in (\overline{\theta}_i, \infty) \end{cases} \quad (25)$$

where $\underline{\theta}_i$ and $\overline{\theta}_i$ denotes the lower and upper bounds of the control parameter θ_i.

Remark 1: For vehicle dynamics, it is feasible to estimate the bounds $[\underline{\theta}_i, \overline{\theta}_i]$ of the control parameters Θ (please refer to [8] for details on this). These bounds can be integrated into the parameter adaptation mechanism using the projection operator as in (25), providing two key benefits. Firstly, the projection scheme can prevent unbounded parameter drift due to noise or disturbances, thereby improving the robustness of the closed-loop adaptive system. Secondly, by restricting the admissible parameter regions with pre-estimated projection bounds, the parameter adaptation process can be improved by avoiding unnecessary learning efforts that occur outside the admissible parameter regions. This enhances the overall effectiveness of the adaptation mechanism.

The $\breve{\theta}_i$ is real-time updated as:

$$\dot{\breve{\theta}}_i = -\gamma_i\mathrm{sgn}(\mathcal{K}_h)|\omega_e|^{s(|\omega_e|)}\mathrm{sgn}(\omega_e)\Psi\mathcal{G}_i - \ell_i. \quad (26)$$

where $\ell_i \triangleq \sigma_i(\breve{\theta}_i - \hat{\theta}_i)$ is a leakage term and,

$$\Psi \triangleq 1 + s(|\omega_e|) + \frac{\partial s(|\omega_e|)}{\partial|\omega_e|}|\omega_e|\ln(|\omega_e|), \quad (27)$$

and $\gamma_i\in\mathbb{R}^+$ is the rate of learning, $\sigma_i\in\mathbb{R}^+$ is the projection operator's rate of leakage (to ensure the boundedness of $\breve{\theta}_i$), and $\mathcal{G}$ is a regressor vector defined as $\mathcal{G} \triangleq (\omega_r \quad \omega_z \quad \varpi_1 \quad \varpi_2)^T$. Moreover, the switching function $s(|\omega_e|)$ is defined as:

$$s(|\omega_e|) \triangleq a + \frac{1}{2}(b-a)\{\tanh[k_s(|\omega_e|-1)]+1\}, \quad (28)$$

where $a\in(0,1)$, $b\in(1,\infty)$, and $k_s\in\mathbb{R}^+$ are design parameters. By design, $s(|\omega_e|)$ is lower bounded by a and is thus positive. It is vital to note that the value of k_s in the switching function should be selected to be large enough to guarantee rapid switching between the values a and b of the function.

Remark 2: The control parameter adaptation law governed by $(26)-(28)$ dynamically speeds up the parameter learning process. Namely, $\dot{\breve{\theta}}_i$ is positively related to the factor $|\omega_e|^{s(|\omega_e|)}$. The value of $s(|\omega_e|)$ switches to b when $|\omega_e|>1$, and to a when $|\omega_e|<1$. On the other hand, the adaptation law for control parameters based on QLF is linear in ω_e in comparison. Thus, the SNQLF design ensures that $|\omega_e|^{s(|\omega_e|)}\mathrm{sgn}(\omega_e)$ is generally greater than $|\omega_e|$, fostering faster learning irrespective of the magnitude of $|\omega_e|$. This dynamically accelerated adaptation can bring about a superior transient response of the closed-loop system. Another important comment to make is that although $\ln(|\omega_e|)$ becomes unbounded when $|\omega_e|$ approaches zero, the value of Ψ stays bounded since $\lim_{|\omega_e|\to 0}|\omega_e|\ln(|\omega_e|) = 0$. To avoid numerical overflow, we can replace $\ln(|\omega_e|)$ with $\ln(|\omega_e|+\nu_s)$ where ν_s is a sufficiently small positive real number. Finally yet importantly, it can be demonstrated that Ψ is always positive if k_s is chosen sufficiently large.

B. Adaptive Closed-loop Stability Analysis

The parameter adaptation error can be compactly denoted as $\widetilde{\Theta} \overset{\text{def}}{=} (\widehat{\Theta} - \Theta)$. The time derivative of the tracking error ω_e (with respect to the reference model) can be succinctly expressed as follows:

$$\dot{\omega}_e = -a_m \omega_e + \mathcal{K}_h \widetilde{\Theta}^T \mathcal{G}. \tag{29}$$

Lemma 2. The following function is lower bounded by zero,

$$V_{\widetilde{\Theta}} \overset{\text{def}}{=} \sum_i \frac{|\mathcal{K}_h|}{2\gamma_i}\left[\left(\breve{\theta}_i - \theta_i\right)^2 - \left(\breve{\theta}_i - \hat{\theta}_i\right)^2\right]. \tag{30}$$

Proof:

If $\breve{\theta}_i \in \left(\underline{\theta}_i, \overline{\theta}_i\right)$, one can see that $\hat{\theta}_i = \breve{\theta}_i$, meaning $V_{\widetilde{\Theta}} = \sum_i \frac{1}{2\gamma_i}\left(\breve{\theta}_i - \theta_i\right)^2$ which is clearly lower bounded by zero.

For $\breve{\theta}_i \notin \left(\underline{\theta}_i, \overline{\theta}_i\right)$, one can re-express $V_{\widetilde{\Theta}}$ in an equivalent form as follows:

$$V_{\widetilde{\Theta}} = \sum_i \frac{|\mathcal{K}_h|}{2\gamma_i}\left(2\breve{\theta}_i - \theta_i - \hat{\theta}_i\right)\left(\hat{\theta}_i - \theta_i\right). \tag{31}$$

If $\breve{\theta}_i \in \left(-\infty, \underline{\theta}_i\right)$, it follows that $\left(2\breve{\theta}_i - \theta_i - \hat{\theta}_i\right) \leq 0$ and $\left(\hat{\theta}_i - \theta_i\right) \leq 0$, thereby implying that $V_{\widetilde{\Theta}}$ is non-negative. On the other hand, if $\breve{\theta}_i \in \left(\overline{\theta}_i, \infty\right)$, we have $\left(2\breve{\theta}_i - \theta_i - \hat{\theta}_i\right) \geq 0$ and $\left(\hat{\theta}_i - \theta_i\right) \geq 0$, which once again leads to the conclusion that$V_{\widetilde{\Theta}}$ is greater or equal to zero. In summary, the fact that $V_{\widetilde{\Theta}}$ is lower bounded by zero is proved. ■

Theorem 2. Respecting the adaptive closed-loop system composed of $(25) - (29)$, one can conclude that $\lim_{t\to\infty} \omega_e(t) = 0$ all the boundedness of all closed-loop signals.

Proof:

First off, an SNQLF is coined as follows:

$$V \overset{\text{def}}{=} |\omega_e|^{1+s(|\omega_e|)} + V_{\widetilde{\Theta}}. \tag{32}$$

It is evident that V is bounded from below by zero (Lemma 1 already establishes the fact that $V_{\widetilde{\Theta}} \geq 0$). The exponent of $|\omega_e|$ adjusts its magnitude dynamically based on the magnitude of $|\omega_e|$, which amounts to a significant shift from the conventional QLF-based adaptive control paradigm wherein this exponent is a constant value.

By the chain rule, we differentiate V with respect to time t, which leads to,

$$\begin{aligned}\dot{V} = \Psi|\omega_e|^{s(|\omega_e|)}\text{sgn}(\omega_e)\dot{\omega}_e + \dot{V}_{\widetilde{\Theta}} = \\ \Psi|\omega_e|^{s(|\omega_e|)}\text{sgn}(\omega_e)\left(-a_m\omega_e + \mathcal{K}_h\widetilde{\Theta}^T\mathcal{G}\right) \\ + \sum_i \frac{|\mathcal{K}_h|}{\gamma_i}\left[\left(\hat{\theta}_i - \theta_i\right)\dot{\breve{\theta}}_i - \left(\breve{\theta}_i - \hat{\theta}_i\right)\dot{\hat{\theta}}_i\right].\end{aligned} \tag{33}$$

By substituting the update law of $\dot{\breve{\theta}}_i$ as stated in $(26) - (27)$ to (33), we have,

$$\begin{aligned}\dot{V} = -a_m\Psi|\omega_e|^{1+s(|\omega_e|)} \\ + \sum_i \frac{|K_h|}{\gamma_i}\left[-\sigma_i\left(\hat{\theta}_i - \theta_i\right)\left(\breve{\theta}_i - \hat{\theta}_i\right) - \left(\breve{\theta}_i - \hat{\theta}_i\right)\dot{\hat{\theta}}_i\right].\end{aligned} \tag{34}$$

It is easy to verify that both $\mathcal{X}$ and $\mathcal{Y}$ as defined in (27) are non-negative. If $\breve{\theta}_i \in \left(\underline{\theta}_i, \overline{\theta}_i\right)$, we have $\breve{\theta}_i - \hat{\theta}_i = 0$ which implies that $\dot{V} = -a_m\Psi|\omega_e| \leq 0$. If $\breve{\theta}_i \in \left(-\infty, \underline{\theta}_i\right)$, it follows from the construction of the projection operator that $\dot{\hat{\theta}}_i = 0$ and $\hat{\theta}_i = \underline{\theta}_i$ as well as $\hat{\theta}_i - \theta_i \leq 0$ and $\breve{\theta}_i - \hat{\theta}_i \leq 0$. Therefore, $\dot{V} \leq -a_m\Psi|\omega_e|^{1+s(|\omega_e|)} \leq 0$. Similarly, if $\breve{\theta}_i \in \left(-\infty, \underline{\theta}_i\right)$, we can infer that $\dot{\hat{\theta}}_i = 0$ and $\hat{\theta}_i = \underline{\theta}_i$ as well as $\hat{\theta}_i - \theta_i \geq 0$ and $\breve{\theta}_i - \hat{\theta}_i \geq 0$, which leads to the same conclusion that $\dot{V} \leq -a_m\Psi|\omega_e|^{1+s(|\omega_e|)} \leq 0$. Summarizing, the conclusion of $\dot{V} \leq -a_m\Psi|\omega_e|^{1+s(|\omega_e|)} \leq 0$ can be reached regardless of the specific values of $\breve{\theta}_i$, which immediately proves the global stability and boundedness of all signals of the closed-loop systems. In addition, it is not hard to show that $\ddot{V}$ is bounded thus inferring the uniform continuity of $\dot{V}$. Therefore, we can conclude that V is lower bounded and $\dot{V}$ is negative semidefinite and uniformly continuous, resulting in $\lim_{t\to\infty}\dot{V}(t) = 0$ and $\lim_{t\to\infty}\omega_e(t) = 0$, as demonstrated by the Lyapunov-like Lemma in [18],[19]. This completes the proof for Theorem 2. ■

Remark 3: If there is a bounded fast-time-varying disturbance d (e.g., wind gusts) presented in the error dynamics (29), the asymptotical convergence of ω_e is lost. Instead, it can only be concluded that ω_e is uniformly ultimately bounded. meaning that it will eventually converge to an invariant set $\chi = \left\{\omega_e \middle| |\omega_e| < a_m^{-1}\bar{d}\right\}$ where $\bar{d} = \max|d|$. Namely, $|\omega_e|$ may drift near zero but is ultimately confined within χ.

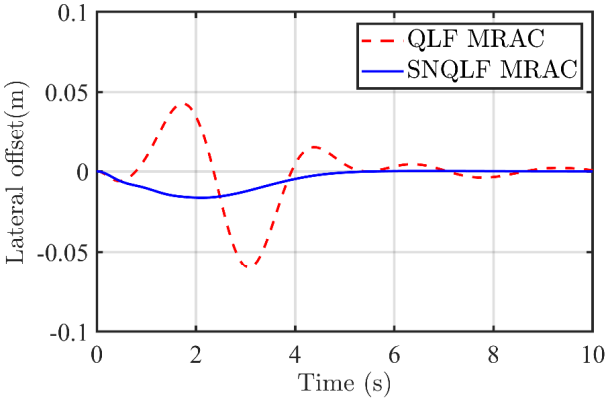

Figure 2. Path-following lateral offset

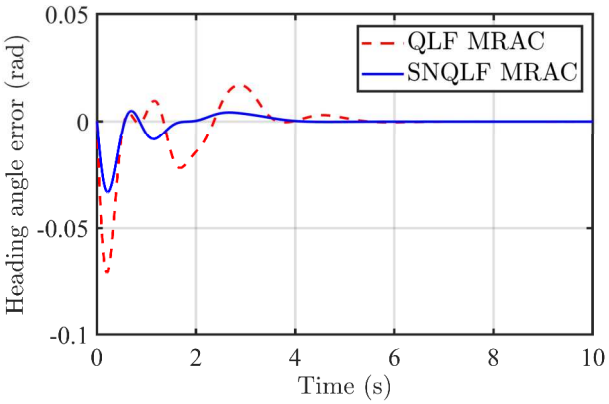

Figure 3. Path-following heading angle error comparison.

V. ASM Simulation Results

The proposed control solution is evaluated through a lane-changing simulation in dSPACE ASM and compared against a baseline QLF-based strategy from [8], with the vehicle's longitudinal velocity ranging between 20 m/s and 30 m/s. The control parameters $\widehat{\Theta}$ are intentionally initialized to be about 25% higher than their actual values Θ (noting that Θ can be computed via the matching condition as derived in [8]), while the projection bounds $\left[\underline{\theta}_i, \overline{\theta}_i\right]$ for these parameters

are set to $\pm 50\%$ of their true values, i.e., $\underline{\theta}_i = 0.5\theta_i$ and $\overline{\theta}_i = 1.5\theta_i$. The gain of the high-level self-scheduled robust H_∞ kinematic error regulator is obtained using the MATLAB LMI solver. To ensure fairness in the comparative study, the SNQLF and QLF MRACs are configured with equivalent learning rates and incorporate identical high-level robust H_∞ controllers. The ASM simulation results displayed in Figures 2 and 3 indicate that, during the transient period, the SNQLF-based MRAC exhibits superior performance over the QLF-MRAC with regard to lateral offset and heading angle error. To be specific, the SNQLF-based MRAC generates a lateral offset that undershoots by less than $0.02\,m$, whereas the QLF-MRAC produces an overshoot that is twice as large. Meanwhile, the SNQLF-based MRAC exhibits significantly less peak error in the heading angle response compared to the QLF-based baseline. The convergence speed of our proposed SNQLF-based solution is significantly faster than the QLF-based baseline counterpart for both error responses, showcasing the superior transient performance of our solution.

VI. Conclusion

This study presents a hierarchical nested-loop control architecture for designing an adaptive path-following controller for automated/autonomous ground vehicles. The proposed design divides the path-following task into kinematic-error regulation and yaw-rate tracking sub-levels. A robust self-scheduled H_∞ controller is developed for kinematic-error regulation and reference yaw rate trajectory generation. A projection-modified SNQLF-based MRAC is synthesized to track the reference command. A Lyapunov-like analysis is conducted to investigate the closed-loop stability, with a focus on proving the asymptotic convergence of the tracking error respecting the reference yaw rate trajectory. The proposed SNQLF-based MRAC is evaluated through dSPACE ASM simulations, showing its superiority over the traditional QLF-based design.

Potential directions for future research could involve testing the proposed control strategy on actual vehicular platforms, such as scaled cars. Additionally, the theoretical results obtained through the SNQLF design could be generalized to other nonlinear systems, providing new insights into the design of adaptive control strategies for a wider range of practical applications.

References

[1] Z. Wang, X. Zhou, and J. Wang, "Extremum-Seeking-Based Adaptive Model-Free Control and Its Application to Automated Vehicle Path Tracking," *IEEE/ASME Trans. Mechatron.*, vol. 27, no. 5, pp. 3874–3884, Oct. 2022, doi: 10.1109/TMECH.2022.3146727.

[2] L. Xiong et al., "IMU-Based Automated Vehicle Body Sideslip Angle and Attitude Estimation Aided by GNSS Using Parallel Adaptive Kalman Filters," *IEEE Trans. Veh. Technol.*, vol. 69, no. 10, pp. 10668–10680, Oct. 2020, doi: 10.1109/TVT.2020.2983738.

[3] A.-T. Nguyen, C. Sentouh, and J.-C. Popieul, "Fuzzy steering control for autonomous vehicles under actuator saturation: Design and experiments," *J. Frank. Inst.*, vol. 355, no. 18, pp. 9374–9395, Dec. 2018, doi: 10.1016/j.jfranklin.2017.11.027.

[4] X. Zhou, Z. Wang, and J. Wang, "Automated Ground Vehicle Path-Following: A Robust Energy-to-Peak Control Approach," *IEEE Trans. Intell. Transport. Syst.*, vol. 23, no. 9, pp. 14294–14305, Sep. 2022, doi: 10.1109/TITS.2021.3126467.

[5] C. Hu, H. Jing, R. Wang, F. Yan, and M. Chadli, "Robust H_∞ output-feedback control for path following of autonomous ground vehicles," *Mech Syst Signal Process*, vol. 70–71, pp. 414–427, Mar. 2016, doi: 10.1016/j.ymssp.2015.09.017.

[6] X. Zhou, Z. Wang, and J. Wang, "Popov-H_∞ Robust Path-Tracking Control of Autonomous Ground Vehicles with Consideration of Sector Bounded Kinematic Nonlinearity," *J Dyn Syst Meas Control*, Jun. 2021, doi: 10.1115/1.4051466.

[7] C. Hu, H. Jing, R. Wang, F. Yan, and M. Chadli, "Robust H_∞ output-feedback control for path following of autonomous ground vehicles," *Mech Syst Signal Process*, vol. 70–71, pp. 414–427, Mar. 2016, doi: 10.1016/j.ymssp.2015.09.017.

[8] X. Zhou, Z. Wang, and J. Wang, "Automated Vehicle Path Following: A Non-Quadratic-Lyapunov-Function-Based Model Reference Adaptive Control Approach With C^∞-Smooth Projection Modification," *IEEE Trans. Intell. Transport. Syst.*, vol. 23, no. 11, pp. 21653–21664, Nov. 2022, doi: 10.1109/TITS.2022.3182928.

[9] T. He, X. Chen, and G. G. Zhu, "A Dual-Loop Robust Control Scheme With Performance Separation: Theory and Experimental Validation," *IEEE Trans. Ind. Electron.*, vol. 69, no. 12, pp. 13483–13493, Dec. 2022, doi: 10.1109/TIE.2022.3140518.

[10] R. H. Byrne and C. T. Abdallah, "Design of a model reference adaptive controller for vehicle road following," *Mathematical and Computer Modelling*, vol. 22, no. 4–7, pp. 343–354, Aug. 1995, doi: 10.1016/0895-7177(95)00143-P.

[11] X. Zhou, Z. Wang, H. Shen, and J. Wang, "Yaw-Rate-Tracking-Based Automated Vehicle Path Following: An MRAC Methodology With a Closed-Loop Reference Model," *ASME Letters in Dynamic Systems and Control*, vol. 2, no. 2, p. 021010, Apr. 2022, doi: 10.1115/1.4053242.

[12] D. Wu *et al.*, "Coordinated Control of Path Tracking and Yaw Stability for Distributed Drive Electric Vehicle Based on AMPC and DYC." arXiv, 2023. doi: 10.48550/ARXIV.2304.11796.

[13] X. Zhou, Z. Wang, H. Shen, and J. Wang, "Robust Adaptive Path-Tracking Control of Autonomous Ground Vehicles With Considerations of Steering System Backlash," *IEEE Trans. Intell. Veh.*, vol. 7, no. 2, pp. 315–325, Jun. 2022, doi: 10.1109/TIV.2022.3146085.

[14] R. Wang, C. Hu, F. Yan, Mohammed Chadli, and N. Chen, "Should the desired vehicle heading in path following of autonomous vehicles be the tangent direction of the desired path?," in *2015 American Control Conference (ACC)*, Chicago, IL, USA, Jul. 2015, pp. 489–494. doi: 10.1109/ACC.2015.7170783.

[15] R. Rajamani, *Vehicle dynamics and control*, 2. ed. in Mechanical Engineering Series. New York, NY Heidelberg: Springer, 2012.'

[16] W. Liu, L. Xiong, X. Xia, Y. Lu, L. Gao, and S. Song, "Vision-aided intelligent vehicle sideslip angle estimation based on a dynamic model," *IET intell. transp. syst*, vol. 14, no. 10, pp. 1183–1189, Oct. 2020, doi: 10.1049/iet-its.2019.0826.

[17] G. E. Dullerud and F. G. Paganini, *A course in robust control theory: a convex approach*. in Texts in applied mathematics, no. 36. New York: Springer, 2000.

[18] E. Lavretsky and K. A. Wise, *Robust and adaptive control: with aerospace applications*. London ; New York: Springer, 2013.